



CuO/La_{0.5}Sr_{0.5}CoO₃ nanocomposites in TWC

G. Carollo^a, A. Garbujo^a, Q. Xin^b, J. Fabro^c, P. Cool^b, P. Canu^c, A. Glisenti^{a,d,*}



^a Dept. of Chemical Sciences, University of Padova, Via F. Marzolo, 1, 35131, Padova, Italy

^b Laboratory of Adsorption and Catalysis, Department of Chemistry, University of Antwerp, Universiteitplein 1, 2610, Wilrijk, Belgium

^c Department of Industrial Engineering, University of Padova, Via F. Marzolo, 9, 35131, Padova, Italy

^d CNR-ICMATE, ISTM, Via F. Marzolo, 1, 35131, Padova, Italy

ARTICLE INFO

Keywords:

TWC
PGMs-free catalysts
Real exhaust mixture
La_{0.5}Sr_{0.5}CoO₃-based nanocomposites
Ammonia driving deposition precipitation (ADP)

ABSTRACT

In this contribution several La_{0.5}Sr_{0.5}CoO₃ based nanocomposites have been prepared and tested for application as Three-Ways Catalysts (TWC), aiming to develop Platinum Group Metal (PGM)-free catalysts. To reach this objective we designed and realized nanocomposites in which active CuO nanoparticles are deposited on La_{0.5}Sr_{0.5}CoO₃. This perovskite is active in oxidation and is characterized by high oxygen anion mobility; copper is active in reduction: catalytic bifunctionality is thus built-in via a tailor-made and controlled nano-composition. The supporting perovskite was prepared following the "citrate" route. The deposition was carried out by means of the Ammonium-Driving-Deposition precipitation (ADP) to highly disperse CuO on La_{0.5}Sr_{0.5}CoO₃. In a precedent paper we focused on nanocomposites obtained using LaCoO₃ as a support because this perovskite is active in oxidation. Sr-doped LaCoO₃, in addition, is characterized by a more relevant presence of oxygen vacancies and mobility and the desire of comparing these systems is to better investigate the different role played by all these aspects on the interaction between highly dispersed CuO nanoparticles and perovskite and on the catalytic activity.

The copper amount on the nanocomposite surface does not increase linearly with the nominal composition reaching a plateau: migration below the surface is observed for the nanocomposite with 30 wt.% of Cu.

The surface composition of the perovskite is modified by the copper deposition which causes the decrease of A-cations surface segregation and enhances the presence of cobalt suggesting a certain synergy; the reducibility of the perovskite is also greatly favored by deposition.

Both model reactions (CO oxidation and CO assisted NO reduction) and reactions with a synthetic automotive exhaust mixture, including 10% steam, and oxygen, were carried out. We compared the results with the ones obtained in similar reactions with CuO/LaCoO₃. Different interaction and synergy were observed with respect to CuO/ La_{0.5}Sr_{0.5}CoO₃. Sr-doping, in fact, enhances oxygen mobility affecting the reducing character of the nanodispersed CuO and thus the reactivity under different conditions.

The deposition of copper oxide significantly increases the activity of the nanocomposites in CO oxidation (about 100% conversion at 200 °C) and in CO + NO (50% conversion at 250 °C, more than 80% at 400 °C) reactions. When compared with the corresponding CuO/LaCoO₃, the more significant difference has been observed in nanocomposites poorer in CuO, which became highly active at lower temperature. On simulated gasoline engine exhaust the nanocomposites always improve the oxidation activity compared to the parent perovskite, while the NO reduction is quantitative in the absence of O₂.

The activity on a mixture simulating actual gasoline-engine exhaust proves that ADP synthesis provides materials with a higher activity compared to wet impregnation (WI), thanks to a higher dispersion of copper. NO reduction in fuel-rich conditions is activated at approx. 300 °C, (400 °C on WI sample), when significant amount of O₂ is still in the mixture. This feature completes the good performance in absence of noble critical metals that are promising facts to develop PGM-free catalysts for the automotive industry.

1. Introduction

LaCoO₃ is known to be a good catalyst for oxidation [1]. The

reactivity of this perovskite can be enhanced by doping, opening to their possible use in Three Way Catalysts (TWCs) free or almost free of noble metals [2–8]. The substitution of Sr(II) for La(III) was observed to

* Corresponding author at: Dipartimento di Scienze Chimiche, Università di Padova, Via F. Marzolo, 1, 35131, Padova, Italy.

E-mail address: antonella.glisenti@unipd.it (A. Glisenti).

increase activity in oxidation of CO, CH₄, C₃H₈ [9], soot [10], and in partial oxidation [11]. Sr(II) doping causes the formation of the redox couple Co(IV)/Co(III) and of oxygen vacancies. L.A. Isupova et al. observed that the content of Sr and the synthesis procedure affect the structure causing rearrangement from hexagonal to cubic back to hexagonal with consequence on reactivity in CO oxidation [12]. La_{1-x}Sr_xCoO_{3-δ} is particularly interesting for oxygen mobility and exchange properties [13–17].

If oxidation can be enhanced by doping, NO reduction is still the more difficult result to be achieved in noble metal free catalysts. In our previous studies, we observed that copper activates NO reduction in perovskites, either increasing oxygen mobility and surface vacancies (when inserted in the lattice) [18] or creating surface active coordinating Cu(II) sites (when deposited on surface, as an example) [19].

Copper containing catalysts are used in a lot of different reactions [20–25]: in all these cases the better performances are obtained when copper is in highly dispersed form [20]. Catalytic systems differing for support, preparation procedure (impregnation, precipitation, etc.), composition, activation treatments (reduction, as an example), can show a different activity and selectivity. In this contribution we selected perovskites as a support at first because these oxides stabilize copper cations avoiding their migration and particles sintering [26].

The reactivity of the nanocomposites, and particularly of dispersed copper species, strictly depends on the specific perovskite: a synergic mechanism involving dispersed copper and perovskite, has to be considered [27]. When the supporting perovskite is LaNiO₃, as an example, NO reduction in complex mixture is favored by H₂ which forms by reforming of hydrocarbons [19]. This behavior was not observed when copper is deposited on LaCoO₃ and NO reduction in complex mixture is low; activity in oxidation (CO, hydrocarbons) is, in contrast, enhanced [28].

To go further in understanding the role played by the interaction between copper active phase and perovskite, in the present contribution the reactivity of copper highly dispersed on Sr-doped LaCoO₃ is considered to evaluate the effect of increasing oxygen mobility in the support on reactivity (in oxidation and reduction).

An innovative deposition procedure, ammonia driven deposition precipitation, was used to deposit highly dispersed copper oxide nanoparticles on perovskites; in this procedure, developed by Guo et al. [29] and optimized for perovskites [19,28], the dispersion is warranted by the formation of copper complexes. The nanocomposites have been carefully characterized by means of X-Ray Photoelectron Spectroscopy (XPS), X-Ray Diffraction (XRD), BET, Temperature Programmed Reduction (TPR), Scanning Electron Microscopy (SEM), and Energy Dispersive X-Ray (EDX) analysis.

The effect of copper oxide deposition on reactivity was studied both in model reactions (CO oxidation and CO assisted NO reduction) and with complex mixtures simulating an automotive exhaust. The mixtures include steam, CO₂ and hydrocarbons: exhaust composition and temperature can severely differ with respect to common laboratory conditions (eg. large NO and CO concentrations, lack of O₂) being extremely challenging to prove the effective activity of the nanocomposites.

The advantages in using ADP, instead of a wet impregnation synthesis (WI), is then discussed. Two samples of 20% Cu on La_{0.5}Sr_{0.5}CoO₃, obtained via ADP and via WI, have been tested both with simple reactions and with the complex mixture simulating actual exhaust. The results have been compared to highlight the contribution of the preparation route.

2. Experimental

2.1. Synthesis

2.1.1. Synthesis of the supporting perovskite

La_{0.5}Sr_{0.5}CoO₃ has been synthesized with the conventional citrate

route [18,30], starting from La₂O₃ (Sigma-Aldrich 99.9%), Sr(NO₃)₂ (Sigma-Aldrich ≥ 98%), and CoO (Acros 99%). The solution was heated at 80 °C in a water bath to promote solvent evaporation and obtain a wet-gel, which was then treated at 400 °C for 2 h in air to decompose the organic framework. The ash-like material was finally grinded and calcined in air at 900 °C (heating rate 6 °C/min) for 6 h to obtain the desired perovskite phase.

2.1.2. Synthesis of the nanocomposites

Cu-loaded La_{0.5}Sr_{0.5}CoO₃ were prepared by the Ammonium-Driving Deposition precipitation (ADP) which was optimized for perovskites [19,28].

Typically, an appropriate amount of Cu precursor (copper nitrate, Cu(NO₃)₂·3H₂O, > 99%, Merck) was dissolved in 10 mL of de-ionized water containing La_{0.5}Sr_{0.5}CoO₃ in order to achieve a final Cu loading of 10, 15, 20 and 30 wt.%. Successively, ammonium hydrate (NH₄OH, 28–30 %, Sigma Aldrich) has been added into the mixture to gain a molar Cu/NH₃ ratio of 1/6. The suspensions were then stirred for 48 h at room temperature, and dried at 60 °C overnight. Finally, the dried samples were calcined at 550 °C (heating rate 1 °C/min) for 8 h. The synthesized catalysts were denoted as 10CLSC, 15CLSC, 20CLSC and 30CLSC, according to the copper loading. The prepared samples are summarized in Table 1.

2.2. Characterization

X-ray diffraction patterns were collected with a Bruker D8 Advance automatic diffractometer, with Cu K α wavelength ($\lambda = 0.154$ nm) at a voltage of 40 kV and a current of 40 mA.

X-ray photoelectron spectroscopy was carried out by means of a ParkinElmer PHI 5600ci Multi Technique System, using AlK α radiation (1486.6 eV) working at 250 W. The spectrometer was calibrated by assuming the binding energy (BE) of the Au 4f_{7/2} line to be 84.0 eV with respect to the Fermi level.

Both extended spectra (survey – 187.85 eV pass energy, 0.5 eV step⁻¹, 0.05 sstep⁻¹) and detailed spectra (for La 3d, Co 2p, Cu 2p, Sr 2p, O 1s and C 1s – 23.5 eV pass energy, 0.1 eV step⁻¹, 0.1 sstep⁻¹) were collected. The standard deviation in the BE values of the XPS line is 0.10 eV. The atomic percentage, after a Shirley-type background subtraction [31] was evaluated by using the PHI sensitivity factors [32]. The peak positions were corrected for the charging effects by considering the C 1s peak at 285.0 eV and evaluating the BE differences [33].

Field emission-scanning electron microscopy and energy dispersive x-ray spectroscopy measures were carried out on a Zeiss SUPRA 40 V P. Both morphological and compositional analyses were carried out setting the acceleration voltages at 20 kV.

The samples for XPS and SEM/EDX have been analyzed in powder form sticking them on Ultra High Vacuum conductive bi-adhesive tape.

The TPR measurements were carried out with an Autochem II 2920 Micromeritics, equipped with a TCD detector in a quartz reactor by using 50 mg of sample and heating from RT to 900 °C at 10 °C min⁻¹

Table 1

Cu/Co atomic ratios, as a function of the nominal composition for the Cu@La_{0.5}Sr_{0.5}CoO₃ nano-composites obtained by Ammonium-Driving Deposition Precipitation (ADP).

Sample	Sample name ^a	Cu/Co ^b
La _{0.5} Sr _{0.5} CoO ₃	LSC	
10% wt. Cu on La _{0.5} Sr _{0.5} CoO ₃	10CLSC	0.41
15% wt. Cu on La _{0.5} Sr _{0.5} CoO ₃	15CLSC	0.56
20% wt. Cu on La _{0.5} Sr _{0.5} CoO ₃	20CLSC	0.80
30% wt. Cu on La _{0.5} Sr _{0.5} CoO ₃	30CLSC	1.15

^a short name used in this article.

^b nominal, from precursors' weighted amounts.

Table 2

Feed composition of all the measurements ($\Lambda = \text{O}_2 \text{ fed}/\text{O}_2 \text{ stoich} = [\text{O}_2]/(0.5[\text{CO}] + 0.5[\text{H}_2] + 2[\text{CH}_4] + 4.5[\text{C}_3\text{H}_6] + 5[\text{C}_3\text{H}_8] - 0.5[\text{NO}])$). For GHSV we assumed a bulk density of all the powders 1 g/ml.

Inert	CO_2	H_2O	O_2	CO	NO	H_2	CH_4	C_3H_6	C_3H_8	Λ	m_{cat}	Flow rate	GHSV	
(balance)	%	%	%	%	%	%	Ppm	Ppm	ppm			mg	Sml/min	1/h
Ar	-	-	-	4	4	-	-	-	-	-	40	100	150000	
Ar	-	-	2	4	-	-	-	-	-	1.0	Stoich	40	100	150000
He	15	10	0.777	0.7	0.1	0.233	230	450	230	1.0	Stoich	200	200	60000
He	15	10	0.609	0.9	0.1	0.300	300	600	300	0.6	Rich	200	200	60000

under a constant flow of H_2 at 5% in Ar (50 ml·min $^{-1}$). TPR samples were previously outgassed with He (50 ml·min $^{-1}$) at RT. The surface area of all samples was determined by Autochem II 2920 Micromeritics. The measurements were carried out at liquid nitrogen temperature (77 K). The specific surface area was calculated using the Brunauer-Emmet-Teller (BET) equation. Prior to N_2 -sorption, all samples were degassed at 200 °C for 16 h.

2.3. Catalytic tests

Two series of catalytic activity tests were carried out, at atmospheric pressure. All the inlet composition and GHSV data are summarized in Table 2 (no inert is used and catalyst fraction is 100%). The first set of measurements is based on simplified mixtures and a quartz reactor (6 mm ID) with a packed bed of powders is used; the temperature was monitored by a thermocouple right upstream of the bed. In this configuration two model reactions have been investigated: NO + CO and CO + O_2 (stoichiometric mixtures). The inert carrier was always Ar. The flow rates were controlled by thermal mass flow meters (Vögtlin Instruments). The temperature of the bed was varied between RT and 400 °C. The composition of the gas mixture (before and after reaction) was measured by GC (Agilent 7890A), with a TCD detector and 13X (60/80 mesh, 1.8 m) and Porapak Q (1.8 m) columns.

The second set of catalytic activity measurements aimed at approaching actual conditions of an automotive exhaust. We used a different quartz flow reactor, 8 mm ID. The experimental set-up has been already described [34]. The gas mixtures were measured by GC (Agilent 7820) with Porapak Q and MS5A packed columns in series; both TCD and FID detectors were used. The GC is online with the gas outlet and programmed to continuously sample the mixture, so that measurements can be collected at approx. 0.1 sample/min. A direct-access, 0-200amu mass spectrometer (Hiden QID-20) was also used to measure NO. The analysis with the MS is almost continuous (0.5–1 sample/min). The flow rates were controlled by mass flow meters (Brooks and Bronkhorst). The feed mixture is a complex one that approximates real automotive exhaust. It is detailed in Table 2. Note that stoichiometry of O_2 is based on the amount required for all the fuels total oxidation plus the amount expected from NO conversion to N_2 and O_2 .

Note that 10% steam was always fed, reflecting actual conditions, quite challenging for the catalysts. The standard testing sequence in the second set of measurements is 1) heating up the catalyst at 10 °C/min to 600 °C in air, 2) 2 h of pre-conditioning at 600 °C in air, 3) 2 h of conditioning at 600 °C with the reacting mixture, 4) slow temperature decrease (−2 °C/min) to measure the catalyst activity at different temperatures, down to 90 °C, a temperature at which any activity is detected. It has been verified that the selected cooling rate of −2 °C/min is sufficiently slow to achieve steady-state operation of the catalyst, at each temperature scanned.

3. Results and discussion

3.1. Chemical, structural, and morphological characterization

Two phases are revealed by the diffraction patterns (Fig. 1): rhombohedral $\text{La}_{0.5}\text{Sr}_{0.5}\text{CoO}_3$ and monoclinic CuO (35.55° and 38.79°).

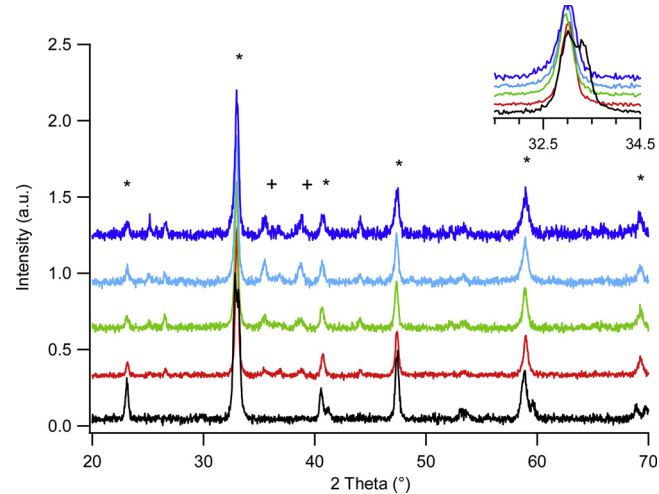


Fig. 1. XRD patterns of the CuO -@ $\text{La}_{0.5}\text{Sr}_{0.5}\text{CoO}_3$ nanocomposites and of the $\text{La}_{0.5}\text{Sr}_{0.5}\text{CoO}_3$ support; from bottom to the top: LSC (black), 10CLSC (red), 15LSC (green), 20CLSC (light blue), 30CLSC (blue) in the insert a detail of the more intense signal of the perovskite.

The absence of shifts toward lower angles in the perovskite signal indicates that Cu did not enter in the unit cell of the perovskite (see insert in Fig. 1).

The deposition of CuO on the $\text{La}_{0.5}\text{Sr}_{0.5}\text{CoO}_3$ is confirmed by the SEM images that reveal the progressive presence of CuO particles with increasing of the CuO deposited amount.

The BET specific surface area does not change significantly as a consequence of the deposition. It is around 4–4.6 m 2 /g for all the nanocomposites, independently on the deposition procedure or copper amount. Only the 30CLSC has a slightly higher surface area (around 7 m 2 /g) (Fig. 2).

La 3d, Sr 3d, Co 2p XPS peak positions are consistent with how expected and not affected by the deposition of Cu. Two overlapping doublets, whose Sr 3d $_{5/2}$ components are centered at about 131.2 and 132.2 eV, are observed; a similar result was obtained by Cheng et al. on $\text{La}_{1-x}\text{Sr}_x\text{CoO}_3$ [35].

The Cu 2p3/2 peaks position (934.0 eV) and shape (shake-up contribution at 942–943 eV) are consistent with $\text{Cu}(\text{II})$ [36]. Two main signals compose the O 1s spectrum of $\text{La}_{0.5}\text{Sr}_{0.5}\text{CoO}_3$: the peak at 528.8 eV is characteristic of the lattice oxygen in metal oxides whereas the one at 531.1 eV is due to oxygen in hydroxides [37–39]. An intense contribution appears at 529.7 eV after copper deposition; the peak position suggests its attribution to CuO .

Beside the higher amount of oxygen, confirming the surface hydroxylation, the XPS quantitative analysis (Table 3) reveals that cobalt is present in slightly higher amount with respect to the nominal value: Co/(La + Sr) XPS atomic ratio being 1.29 instead of 1.00; also the EDX Co/(La + Sr) atomic ratio is higher than nominal 1.23 underlining that Co-surface segregation interests several monolayers. This was not observed in the corresponding $\text{CuO}/\text{LaCoO}_3$; in this case, in fact, the XPS and EDX Co/La atomic ratios were 0.59 and 0.91, respectively (lower than the nominal value). In both cases, copper deposition does not alter

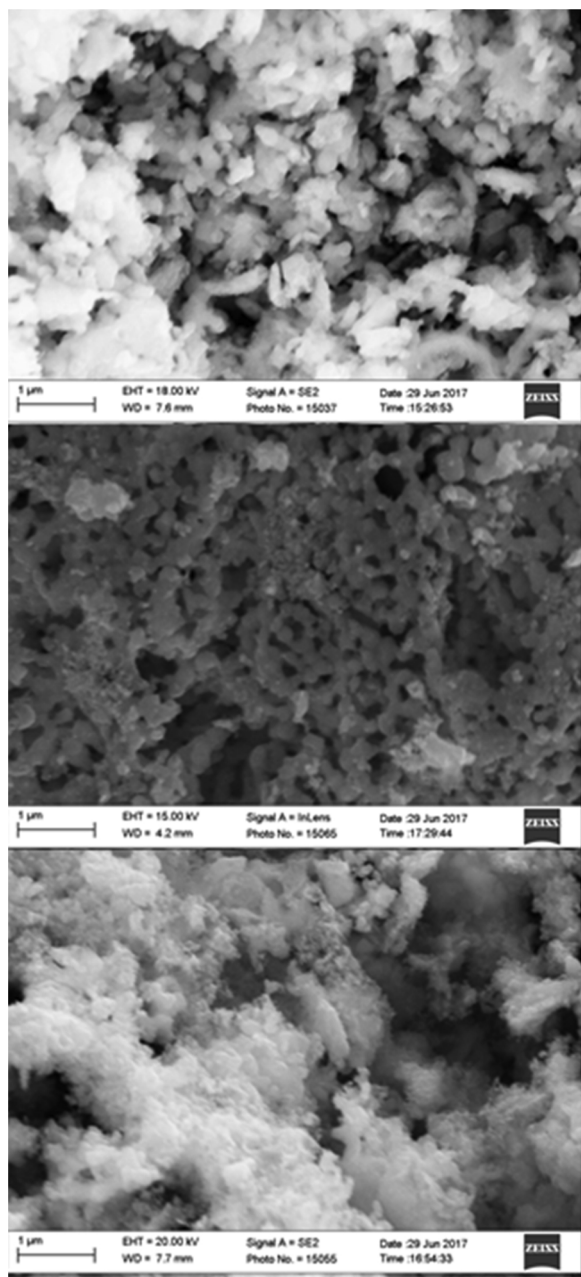


Fig. 2. SEM images of the supporting LSC (upper), 10CLSC (middle), and 30CLSC (lower).

this behavior. Cu/(La + Sr) atomic ratio increases with the amount of copper deposition from 0.29 to 0.88, as expected for a surface deposition procedure; in general, the Cu/(La + Sr) atomic ratio is higher than the corresponding Cu/La atomic ratio observed for the CuO/LaCo₃ nanocomposites; moreover, unlike CuO/LaCo₃ the Cu/(La + Sr) atomic ratio is higher or equal to the nominal one confirming the absence of diffusion toward bulk. A different behavior is revealed by the 30CLSC sample: in this case the Cu/(La + Sr) XPS atomic ratio is 0.88, lower than the nominal one (1.04) and the EDX value is higher (1.54) suggesting that in this case copper tends to diffuse inside the bulk. Also the Cu/Co atomic ratio gives interesting information; in fact, it ranges from 0.48 to 0.60 in 10CLSC, 15CLSC and 20CLSC and is 0.67 in 30CLSC; the Cu/Co atomic ratio in CuO/LaCo₃ is 0.6 in the 15CLC, the more performant catalyst of this serie. The Sr/La atomic ratio is around the nominal one.

3.2. Temperature programmed reduction

H₂-TPR (Fig. 3 - Table 4). Two groups of signals are observed in the supporting LSC: the one around 400–500 °C is due to the reduction Co (III)/Co(II) whereas the contributions at higher temperatures (600–800 °C) to Co(II)/Co(0) [3,40–45]. The rather broad and complex curve observed around 600–900 °C suggests that not equivalent Co(II) sites are induced by Sr doping. A broad band at lower temperature (200–400 °C) is attributed to Co(IV) species; this is confirmed by the agreement between the higher consumption % amount and the % of these contribution in the fitted experimental curves (around 30% of the total signal). It is interesting to observe that this phenomenon is not evident in the un-doped LaCo₃ and when the amount of doping Sr is low (in Fig. 3 the TPR of La_{0.8}Sr_{0.2}CoO₃ is also reported for comparison).

Focusing on the nanocomposites, an intense signal at 200–300 °C appears, consistently with the deposition of CuO. Bulk CuO has, generally, been reported to reduce around 300 °C [19,28,46], 316 °C was the reduction temperature measured in our experimental setup for a commercial sample. The fitting procedure reveals two contributing peaks at 270 and 290 °C; the lower temperature with respect to the commercial CuO is consistent with the dispersion of the deposited oxide. With increasing CuO amount, the relative intensity of the two copper signals (270 and 290 °C) changes (Group 2) and, in particular, the intensity of the signal at 290 °C decreases and that of the peak at 270 °C increases. This behavior is related to the presence of two types of CuO nanoparticles differently interacting with the perovskite surface: smaller particles, characterized by strong interaction with the surface, and bigger particles less interacting with the perovskite and showing a behavior similar to that of bulk CuO. Several studies concerning the effect of dispersion of particles and the interaction with the support on the reducibility of nanocomposites have been published: CuO on mesoporous silica [47,48], cerium and zirconium oxides [49–51], NiO-CeO₂ [52] mesoporous MnO_x-CeO₂ [53], Ce_xSn_{1-x}O₂ [54] Ce_{1-x}Ti_xO₂ [55], Ti_xSn_{1-x}O₂ [56]. Summarizing, different types of copper oxide nanoparticles can be observed (frequently named α , β , γ) and are rationalized as a function of increasing reduction temperature: isolated Cu²⁺ ions strongly interacting with the support, small two- and three-dimensional clusters of loose structures that have no specific and regular lattice arrangement; large three-dimensional clusters and bulk CuO phase that have characters and properties identical to those of pure CuO powder. Luo et al. [57] attributed the three reduction peaks to finely dispersed CuO, Cu²⁺ ions in Cu_xCe_{1-x}O₂ solid solution, and bulk CuO. With increasing the amount of deposited copper the number of particles characterized by lower dimension increases whereas the contribution of the bigger ones, decreases. This behavior was not observed when depositing, by mean of ADP, CuO on LaCo₃ (in this case a reduction temperature typical of bulk CuO was observed – [28]) and has thus to be attributed to the La_{0.5}Sr_{0.5}CoO₃ support.

Dow and Huang [58] studied the effect of oxygen vacancies on the interaction between CuO and Yttria Stabilized Zirconia (YSZ) until 500 °C under reducing and oxidizing conditions. They observed that when CuO is supported on alumina, the nanocomposite surface energy can be decreased with the formation of copper aluminates, a behavior enhanced by the high specific surface area of alumina. On YSZ, characterized by low surface area and porosity, under reducing conditions copper can migrate on surface and coalesce; when oxygen surface vacancies are present copper species can drop into vacancies reducing surface energy (metal nesting). The temperature favors the penetration of reduced copper into the support and the development of a tensile strength that causes the formation of cracks and splits copper particle into smaller ones. Re-oxidation may not be sufficiently effective to cause the re-migration of copper toward the surface. The comparison between LaCo₃ and La_{0.5}Sr_{0.5}CoO₃ reveals that Sr-doping causes the increment of oxygen vacancies [13–16,59] so greatly facilitating the migration of copper species (as confirmed by the XPS and EDX

Table 3

XPS and EDX atomic compositions obtained for the $\text{Cu}@\text{La}_{0.5}\text{Sr}_{0.5}\text{CoO}_3$ nanocomposites; inside brackets the atomic composition determined considering only the cations are reported to underline the segregation/diffusion phenomena. The nominal compositions (from the weighted amounts) are reported for comparison.

Sample		La	Sr	Co	Cu	O	Co/(La + Sr)	Sr/La	Cu/Co	Cu/(La + Sr)
$\text{La}_{0.5}\text{Sr}_{0.5}\text{CoO}_3$	XPS	8.5 (26.2)	6.3 (19.6)	17.5 (54.1)	–	67.7	1.29	1.05	–	–
	EDX	11.5 (22.6)	11.3 (22.3)	28.0 (55.1)	–	49.1	1.23	0.99	–	–
	Nominal	10 (25.0)	10 (25.0)	20 (50.0)	–	60.0	1.00	1.00	–	–
10CLSC	XPS	7.0 (20.5)	5.6 (16.3)	14.7 (42.7)	7.1 (20.6)	65.7 (20.6)	1.16	0.79	0.48	0.29
	EDX	7.6 (18.1)	9.0 (21.4)	17.6 (41.8)	7.9 (18.7)	58.0	1.06	1.19	0.45	0.47
15CLSC	Nominal	8.9 (21.6)	8.9 (21.6)	18 (43.2)	6 (13.6)	58.9	1.00	1.00	0.32	0.32
	XPS	6.1 (20.0)	5.5 (18.0)	12.9 (42.2)	6.1 (19.8)	69.4 (54.3)	1.11 (1.09)	0.90 (1.05)	0.47 (0.28)	0.52 (0.32)
20CLSC0	EDX	9.3 (20.3)	9.7 (20.3)	20.8 (45.5)	5.9 (12.9)	54.3	1.09	1.05	0.28	0.32
	Nominal	8.3 (19.8)	8.3 (19.8)	16.6 (39.7)	8.6 (20.6)	58.3	1.00	1.00	0.52	0.52
30CLSC	XPS	5.5 (15.9)	5.8 (16.7)	14.6 (42.0)	8.8 (25.3)	65.4 (51.8)	1.29 (1.11)	1.05	0.60	0.78
	EDX	9.1 (19.0)	9.3 (19.4)	20.4 (42.4)	9.3 (19.2)	51.8	1.11	1.02	0.45	0.50
Nominal	Nominal	7.8 (18.6)	7.8 (18.6)	15.7 (37.1)	10.8 (25.7)	57.8	1.00	1.00	0.69	0.69
	XPS	5.1 (14.8)	5.6 (16.3)	14.3 (41.3)	9.5 (27.5)	65.5 (52.3)	1.33 (1.17)	1.10	0.67	0.88
Nominal	EDX	6.6 (13.8)	6.3 (13.2)	15.0 (31.5)	19.8 (41.5)	52.3	1.17	0.95	1.32	1.54
	Nominal	7.1 (16.4)	7.1 (16.4)	14.1 (32.9)	14.7 (34.2)	57.1	1.00	1.00	1.04	1.04

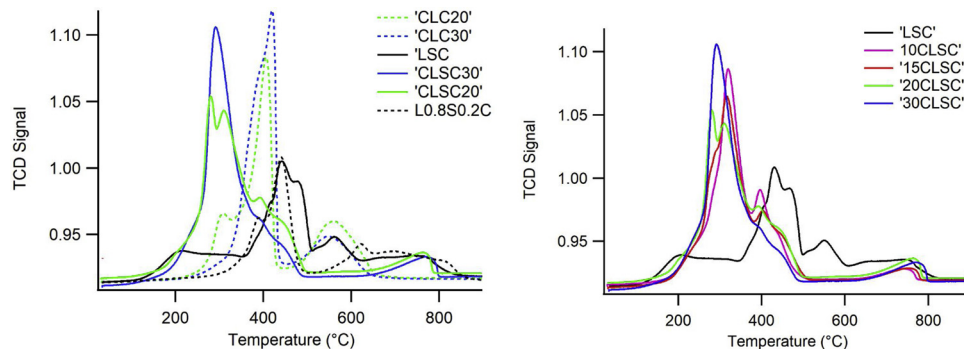


Fig. 3. $\text{H}_2\text{-TPR}$ graphs obtained for the supporting LaSrCoO_3 (black) and for the nanocomposites 10CLSC (red), 15CLSC (green), 20CLSC (light blue), 30CLSC (blue); for comparison the signals of the LSC support containing lower amount of Sr (0.2 instead of 0.5) is reported (bold line) as well as the corresponding data obtained by depositing copper on LaCoO_3 (CLC); left: effect of support copper oxide deposited on LC and LSC; right: effect of the increasing copper deposition on LSC.

Table 4

TPR H_2 consumption data determined on $\text{La}_{0.5}\text{Sr}_{0.5}\text{CoO}_3$ and on the nanocomposites obtained by depositing CuO by ADP (CLSC); the consumption values are compared with the expected ones (calculated considering Co(III) and Cu(II)). The values concerning $\text{La}_{0.8}\text{Sr}_{0.2}\text{CoO}_3$ are also reported for comparison.

Sample	H_2 [mol/mole] Measured	H_2 [mol/g] Expected ^a	GROUP 1 Co(IV)/Co(III)	GROUP 2 Cu(II)/Cu(0)	GROUP 3 Co(III)/Co(II) Co(II)/Co(0)	GROUP 4 Co(II)/Co(0) %
LSC ($\text{La}_{0.5}\text{Sr}_{0.5}$)	1.863	1.500	0.428 23	0.000	0.987 53	0.447 24
LSC ($\text{La}_{0.8}\text{Sr}_{0.2}$)	1.654	1.500	0.000	0.000	1.277 77	0.377 23
10CLSC	1.585	1.371	0.214 14	0.258 16	1.114 70	
15CLSC	1.540	1.329	0.211 14	0.342 22	0.987 64	
20CLSC	1.515	1.295	0.220 15	0.409 27	0.886 58	
30CLSC	1.452	1.245	0.207 14	0.502 34	0.753 52	

compositional data) and the formation of small copper particles. The peak attributed to Co(III)→Co(II) reduction remains essentially at the same temperature but, noteworthy, the contribution due to Co(II)→Co(0) reduction disappears and consumption data suggest that all cobalt is reduced around 400–450 °C. The attitude of copper to induce the reduction of cobalt at lower temperature was already observed in literature both when copper is a dopant inside the perovskite cell [18,34] and when it is deposited on the surface [19,28]. Tien-Thao et al [60,61] hypothesized that highly dispersed elemental copper formed under TPR conditions, can act as a catalyst for hydrogen dissociation. This causes the decrease of the cobalt reduction temperature, particularly for grain boundaries cobalt species. This phenomenon was observed to be even more evident when CuO is deposited on the perovskite surface in a highly dispersed form [19,28] and is thus reasonable that it is more effective when highly dispersed copper migrates inside the material grain.

A small signal at around 750 °C is evident; Onrubia et al. [62], by investigating $\text{La}_{1-x}\text{Sr}_x\text{CoO}_3$ catalysts with TPR and mass quadrupole could attribute this to the decomposition of carbonates.

The H_2 consumption values are compared in Table 4 with the ones calculated considering the presence of Cu(II) and Co(III). The values obtained for the total consumption are always higher than the calculated ones, suggesting the presence of cations in higher oxidation state. The determined difference is always around 30–40% of the molar amount of cobalt suggesting its attribution to the presence of cobalt in higher oxidation state (the presence of Co(IV) also agrees with the low temperature broad band observed, moreover no significant trend was observed as a function of the molar content of CuO, as an example). The deposition of copper, beside decreasing the reduction temperature, promotes cobalt reduction to oxidation states lower than Co(II) at 400–500 °C, as revealed by the absence of the signal at higher temperature (named Group 3). This behavior was already observed in copper containing cobaltates both when copper is inside the perovskite structure and when it is surface deposited.

3.3. Catalytic activity

3.3.1. Reactivity in $\text{CO} + \text{O}_2$

Fig. 4 (top panel) compares the CO conversion achieved, as a function of temperature, with $\text{La}_{0.5}\text{Sr}_{0.5}\text{CoO}_3$ and the nanocomposites. Almost complete conversion (> 90%) has been always achieved at temperatures higher than 250 °C. The copper oxide deposition significantly affects the ignition, that occurs at lower temperature than just LSC, above 100 °C, and the oxidation rate, that gradually increases with temperature, compared to the abrupt ignition shown by LSC, between 200 and 250 °C. At 200 °C, the effect of copper oxide deposition is well evident; up to 20% Cu deposited, there is a positive increase of oxidation rate, up to 100% conversion. Consistently with the copper migration mechanism revealed by XPS/EDX and TPR, the sample with 30% copper oxide loading is less active than samples at lower loading, but still better than just LSC. The support is almost inactive below 200 °C.

Considering the chemisorptive character of CO it can be supposed that it prefers to adsorb on p-type semiconducting oxides, such as Cu_2O that facilitate the donor-type reaction of CO [58]. TPR results indicate that around 200 °C the Cu(II) reduction starts, and thus the formation of CO chemisorption sites. In general, the CO oxidation is expected to follow a Mars-van Krevelen mechanism with the catalyst providing to the chemisorbed CO, the active oxygen restored successively by the reacting mixture [63]. Another hypothesis, suggests the possible intervention of activated surface species formed by interaction of molecular oxygen with surface oxygen vacancy sites [56]. Fierro et al. reported a mechanism consistent in the chemisorption of CO on surface oxygen atom to form carbonates and then carbon dioxide [64]. In a work carried out by some of the authors [65], CO oxidation was studied by a pulses approach revealing that bulk oxygen intervention into the reactivity strongly affects the activation energy and the Oxygen

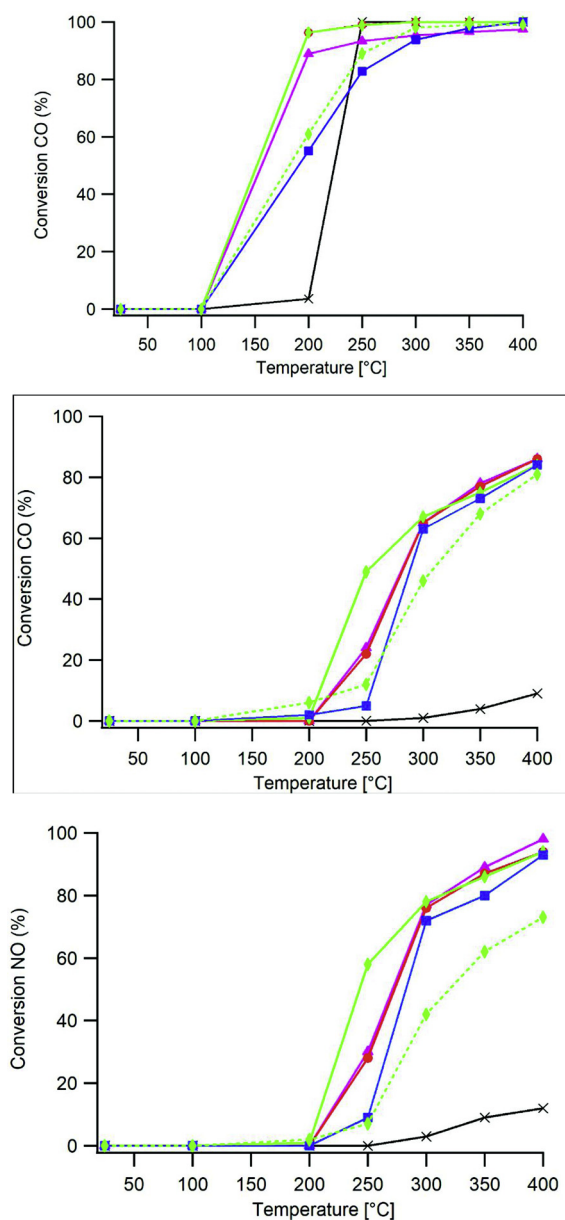


Fig. 4. CO and NO conversion as a function of temperature obtained for $\text{La}_{0.5}\text{Sr}_{0.5}\text{CoO}_3$ (black crosses) and $\text{Cu}@\text{La}_{0.5}\text{Sr}_{0.5}\text{CoO}_3$ (rose triangles) 10CLSC, red ball 15CLSC, green rhombus 20CLSC, blue squares 30CLSC) in the CO oxidation (upper graph) and in the CO assisted NO reduction. The conversion values obtained for a nanocomposite 20CLSC prepared by wet impregnation (dotted line), are also reported.

Exchange Capability. Bulk oxygen intervention depends on doping (being highly favored by Sr in contrast to Cu-doping or with the undoped LaCoO_3) and on temperature (beginning to be significant around 300–350 °C). These results suggest that, in the present case, the reaction ignition is to be attributed to the formation of interfacial Cu_2O which is stabilized on the surface of the perovskites characterized by lower copper amounts (the high Oxygen Exchange Capability of $\text{La}_{0.5}\text{Sr}_{0.5}\text{CoO}_3$ with respect to LaCoO_3 being already mentioned).

3.3.2. Reactivity in $\text{CO} + \text{NO}$

The catalytic tests with $\text{CO} + \text{NO}$ mixtures were performed using stoichiometric amounts of CO and NO, each at 4% dilution (see Table 2). The results are compared in Fig. 4 (lower panels). The supporting $\text{La}_{0.5}\text{Sr}_{0.5}\text{CoO}_3$ shows very low activity, even at 400 °C.

Again, and more effectively, the catalytic performance on CO

oxidation and NO reduction is greatly enhanced by copper oxide deposition. Also in this reaction we observe a progressively positive effect of the copper amount, until 20%, while the highest loading is less active, but still well above the support. A common light-off temperature > 200 °C is observed as well as conversions approaching 90% at 400 °C. The effect of temperature on conversion reflects different controlling steps at ignition (between 200 and 300 °C) and at higher temperature (> 300 °C), where the increase of conversion rate with temperature is less effective.

We can certainly attribute the difference to a chemical mechanism, rejecting the hypothesis of diffusion control; indeed, the results in the oxidation reaction (Fig. 4 top panel), collected in the same bed geometry, at the same flow rate, clearly prove that 100% conversion can be achieved with a fast reaction, without any diffusion limitations. The results of both reactions suggest that an optimized composition is needed to achieve the maximum catalytic activity. A synergic effect of copper and perovskite surface may also be strictly involved in the reactivity, so an excessive deposition or coverage of the support does not appear so effective. It has to be considered, however, that also the Cu/Co atomic ratio is relevant.

In fact, the ratio is around 0.5–0.6 in the samples 10CLSC to 20CLSC and the contribution due to the CuO particle more strongly interacting with the surface is relevant whereas in the sample 30CLSC the less interacting particles are prevalent and the Cu/Co is around 0.67. These results suggest that a strong interaction between CuO nanoparticles highly dispersed and perovskite is necessary for the catalyst to be active.

The CO and NO conversions obtained at different temperature as a function of Cu loading are compared in Fig. 5. A very high oxidation activity at 250 and 400 °C is proved by all the samples, independently on the presence of copper, including La_{0.5}Sr_{0.5}CoO₃ (0% wt.). Copper deposition greatly favors the catalytic activity at 200 °C that increases from 3 to about 90%. Similar results are obtained at 15 and 20 wt. % but it is relevant that the catalytic activity tends to decrease (at 55%) for the higher Cu loading (30 wt. %). This behavior is consistent with the observed migration of copper inside the grains (XPS, TPR). NO reduction is not observed until 250 °C and also in this case Cu increases activity from about 0% to 30% at 250 °C and from 12 to 98% at 400 °C.

The mechanism proposed in literature for CO + NO reaction over several perovskite surfaces, among which cobaltates, takes into consideration several steps [66–70]:

adsorptions

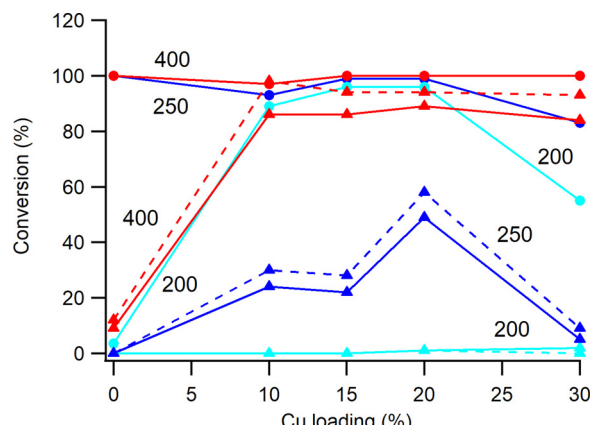
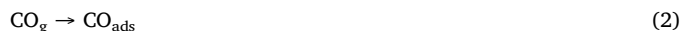
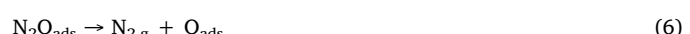


Fig. 5. Comparison among the CO (continuous line) and NO conversions (dashed line) in CO oxidation (●) and CO + NO reaction (▲) as a function of Cu loading (wt. %) at increasing temperatures: 200 °C (light blue), 250 °C (blue), and 400 °C (red).

surface reactions



desorptions



Taking into consideration the adsorption steps (1 and 2), several authors observed that CO affinity toward the surface of LaCoO₃-based perovskites is weaker than that of NO and that CO preferentially interacts with cobalt cations [66,71,72].

At low temperatures the dissociative chemisorption of NO is the Rate Determining Step (RDS) of the catalytic reduction of NO by CO on perovskites, and particularly on copper containing lanthanum cobaltates (steps 3 and 4) [66]; the availability of active sites is determinant. In perovskites, the interaction of NO with a surface oxygen vacancy, provides enough energy for the N–O bond breakage; doping with elements capable of enhancing oxygen vacancy formation, mobility toward surface and stability, is strategic [18,73,74].

Beside oxygen vacancies, copper cations can play a role: they are expected to coordinate two NO molecules forming a dinitrosyl specie that decomposes forming N₂ and/or N₂O [66,73]. The NO dissociation can also involve the formation of the dimeric species (N₂O₂) as intermediate; in this case the formation of N₂O is much easier only involving a N–O bond breaking whereas the formation of N₂ should result from two bonds cleavages. In nanocomposites obtained, as in the present case, by depositing CuO on the surface of perovskites, the role played by oxygen vacancy is, probably, to stabilize interfacial Cu₂O, which is the active specie in NO coordination; CO coordination, in contrast, is consistent with the cobalt surface segregation, revealed by XPS. The presence of sites active for the coordination of CO and NO favours the surface reaction (steps 3 to 7). At this purpose it is relevant to observe that in the CuO/LaCoO₃ nanocomposites the activity in CO assisted NO reduction requires higher temperatures and higher copper amounts (NO conversion to N₂ being less than 50% in 10% wt. CuO/LaCoO₃ catalyst and 30% wt. CuO/LaCoO₃ is required to have 100% conversion at 400 °C); this can be related to the absence of oxygen vacancies capable of stabilizing copper as Cu₂O.

Comparing the conversion results it appears that in almost all cases there is not a significant difference between the activity of the samples with 10–20 wt. % but for CO assisted NO reduction the catalyst with 20 wt. % seems better. Because of this reason 20CLSC was selected to be tested with the complex mixture and for a more accurate comparison with a correspondent sample obtained by wet impregnation. In this last case the conversion values determined both for CO oxidation and for CO assisted NO reduction (Fig. 4) are always lower confirming the relevance played by the high dispersion on activity.

3.3.3. Catalytic activity: Reactivity with a synthetic automotive exhaust

The positive results achieved on simple reactions by the nanocomposites, compared with the simple LSC, supported the additional effort of a more realistic testing of them, on a complex mixture approaching the automotive (gasoline) exhaust (Table 2).

The comparative activity of 20% copper loaded nanocomposites with a stoichiometric mixture is reported in Fig. 6. Data of 20%CuO on La_{0.5}Sr_{0.5}CoO₃ are compared with the simple LSC. Our previous measurements [28] on LaCoO₃ and Cu@LaCoO₃ at comparable loading are

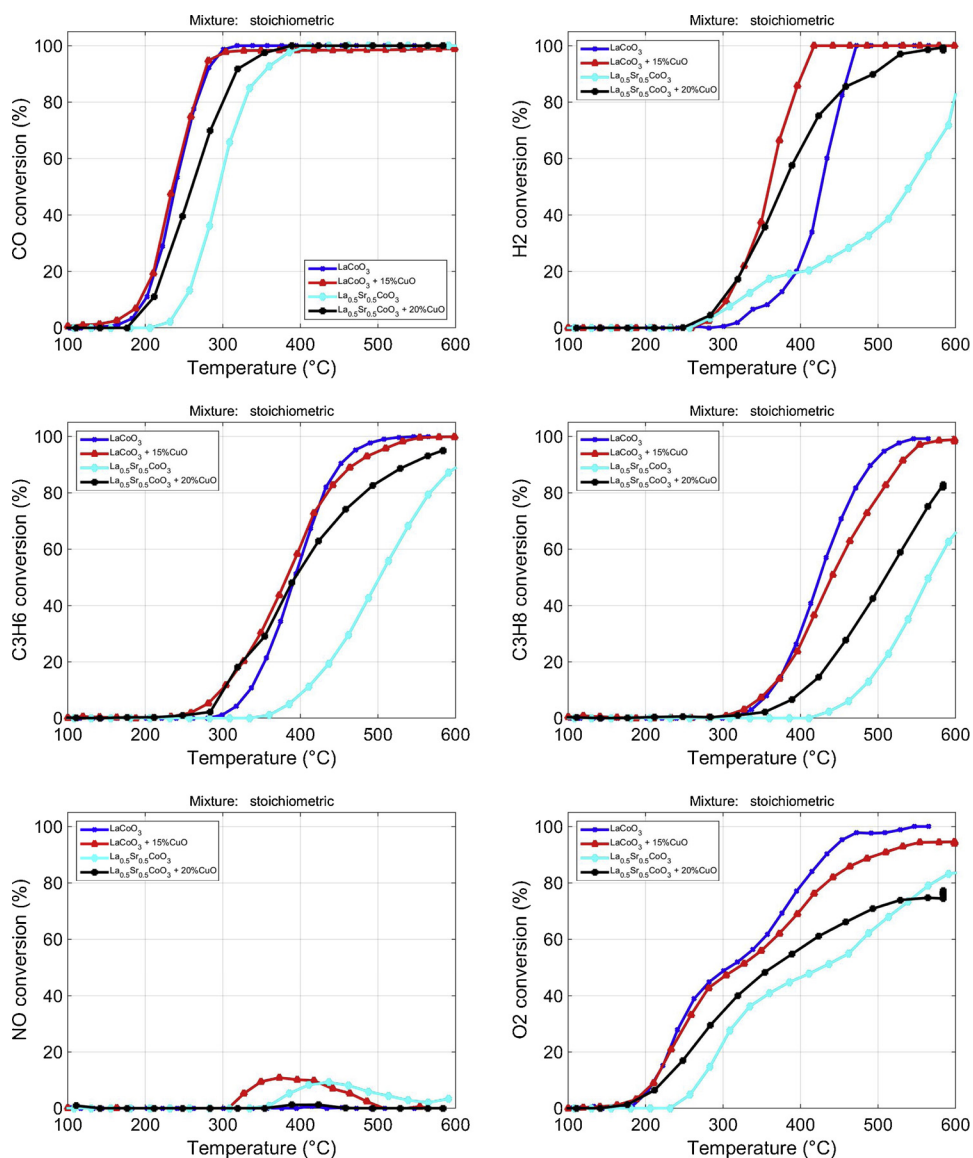


Fig. 6. Single reactants' conversion as a function of temperature, feeding a stoichiometric complex mixture (See Table 2) on $\text{La}_{0.5}\text{Sr}_{0.5}\text{CoO}_3$ and its 20%CuO composite. Previous data of LaCoO_3 and 15%CuO on LaCoO_3 [28] are also reported for comparison.

also reported in the same Figure. Thanks to a higher sampling rate during temperature increase, we can clearly identify that CO oxidation on $\text{Cu}@\text{La}_{0.5}\text{Sr}_{0.5}\text{CoO}_3$ is significantly anticipated by more than 50 °C, with respect to the bare LSC, now starting below 200 °C. Complete conversion, is achieved at 350 °C, quite a low temperature, suitable for automotive applications. Note that CO oxidation activity of Sr-doped cobaltate with the addition of CuO approaches the activity of LaCoO_3 (where the CuO effect was negligible). The improvement in H_2 conversion is very remarkable, closely approaching the LaCoO_3 composite. It is expected that reduced copper can catalyze H_2 dissociative chemisorption enhancing its conversion.

Hydrocarbons oxidation requires a higher temperature than CO, above 300 °C, depending on the species stability. Propene start burning even below 300 °C, propane above 350 °C, while methane (not shown) start oxidizing close to 500 °C, to a very limited extent (10% conversion at 600 °C). As expected, the large amount of O_2 available at stoichiometric conditions strongly limits the reduction of NO, confirming the roles played by oxygen vacancies in NO activation and in stabilizing the Cu_2O specie. The profile of O_2 consumption on $\text{Cu}@\text{La}_{0.5}\text{Sr}_{0.5}\text{CoO}_3$ confirms the approach to the activity of LaCoO_3 and its composite, confusing low- and high-temperature oxidations that were so clearly

separated on LSC, and also on LaCoO_3 and its composite.

The comparison of the activity of the same samples in oxygen deficient (fuel rich) mixture is reported in Fig. 7. At the cost of some lowering of the CO oxidation effectiveness, still not affecting the low ignition temperature (approx. 200 °C), the oxidation of H_2 and propane is greatly enhanced. Oxidation activity always approaches that of the CuO composite on un-doped LaCoO_3 ; however, comparable performances are now achieved with half of the La amount. Propene oxidation remains always scarce at fuel-rich condition on LSC, and slightly worse with the composite. That is explained by the total consumption of O_2 below 400 °C that limits the oxidation of the hydrocarbons surviving that temperature; besides the limited propene conversion mentioned, also methane is essentially unconverted (data not shown).

The most relevant result is the NO conversion, that can now be achieved below 350 °C on the composite, up to almost total reduction at high temperature, providing this functionality to the bare LSC, that was unable to support any NO reduction, even at high temperature. The successful, quantitative reduction of NO is facilitated by the total consumption of O_2 . Results confirm the known trade-off between oxidation and reduction features of the catalyst, where the latter requires the oxygen to be consumed before activating. This is consistent with the

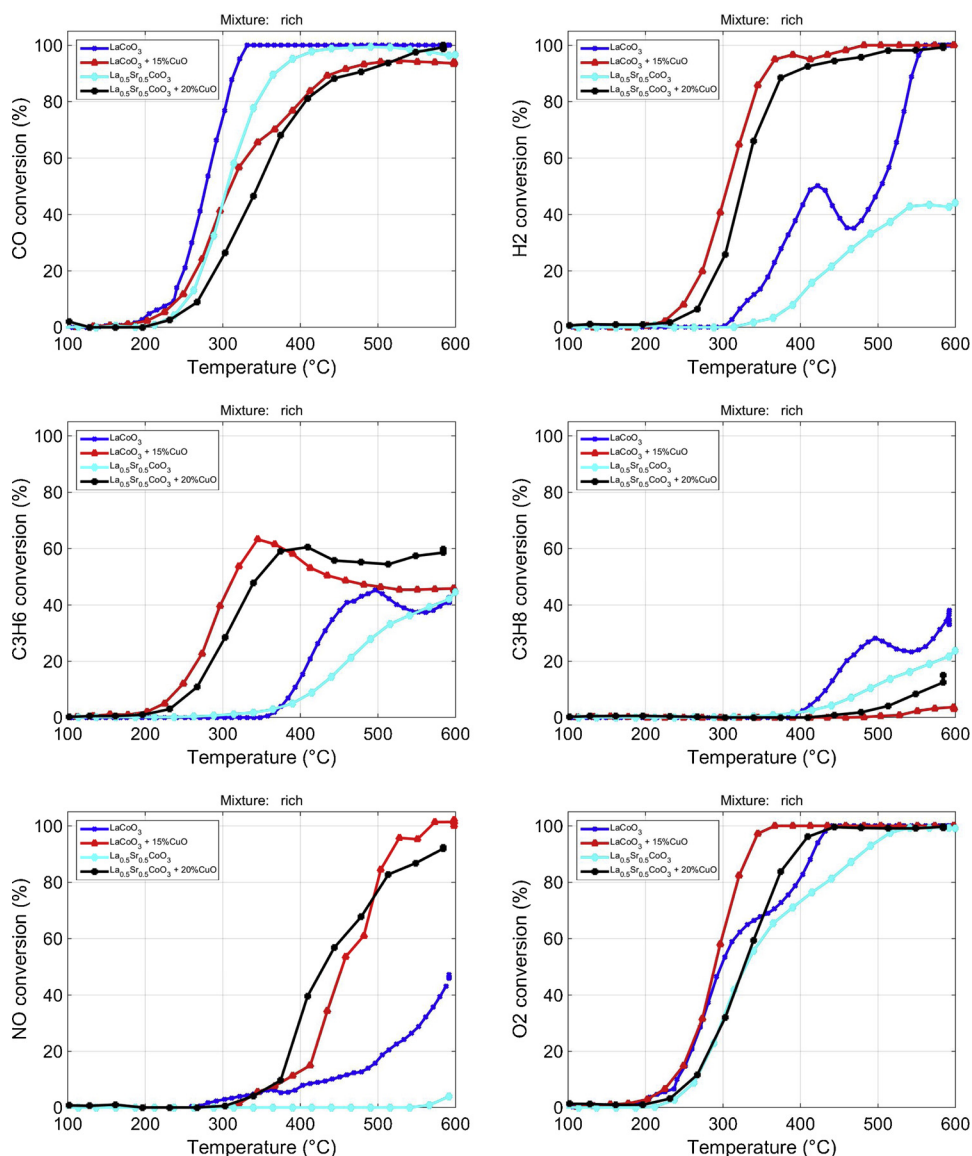


Fig. 7. Single reactants' conversion as a function of temperature, feeding a fuel-rich complex mixture (See Table 2) on 10, 15, 20% copper oxide loading on La_{0.5}Sr_{0.5}CoO₃.

already mentioned need of reduced copper species to obtain a successful coordination of NO.

We also compared the method of synthesis. The reactivity of two samples of 20% CuO on La_{0.5}Sr_{0.5}CoO₃, obtained via ADP or via WI, has been evaluated, feeding the complex mixture of Table 2, in addition to the simpler CO oxidation and CO-assisted NO reduction presented in Fig. 4. The catalytic activity of the material prepared by ADP is always higher than the corresponding one obtained by WI, as shown in Figs. 8 and 9.

At stoichiometric conditions, Fig. 8, the ignition temperature for the oxidation of CO, H₂ and hydrocarbons on samples prepared by ADP is lower by 20–50 °C. Notwithstanding the misleading appearance of this representation of data, in the light-off region the catalyst synthesized by ADP are significantly more active in any oxidation; improvements in conversion, at given temperature, range between 10–30% for CO, compared to the WI sample. Methane conversion is again barely affected (data not shown). NO reduction is confirmed to be penalized by the presence of oxygen, not totally consumed.

In fuel-rich conditions, Fig. 9, the positive results with the ADP sample are confirmed. The extent of CO and H₂ oxidation is always larger compared with the WI catalyst, at the same temperature.

Interestingly, the latter seems to promote the production of H₂ (drop of conversion) above 400 °C, when O₂ is lacking; the data suggest C₃H₈ dehydrogenation, with C₃H₆ production, competing with its consumption. The same mechanism is not evident on the ADP catalyst. The most interesting feature achieved with the latter catalyst is the dramatic enhancement of NO reduction, activated at 300 °C, i.e. 100 °C lower than WI catalyst. At 300 °C the oxygen conversion is quite limited (approx. 30%) since the oxidations are still kinetically limited; thus, the ability of the ADP catalyst to promote the reduction of NO in presence of a relatively large amount of oxygen is very interesting. Furthermore, the activation energy of reduction on the ADP sample appears significantly lower than on the WI one, showing a large consumption of NO when kinetic regime controls. At 450 °C the conversion is more than doubled in ADP sample compared to the WI one.

The present results confirm again the enhanced dispersion of copper provided by ADP improves the reactivity of 20% CuO on La_{0.5}Sr_{0.5}CoO₃ catalyst as TWC, especially at conditions closer to the actual gasoline engine exhaust.

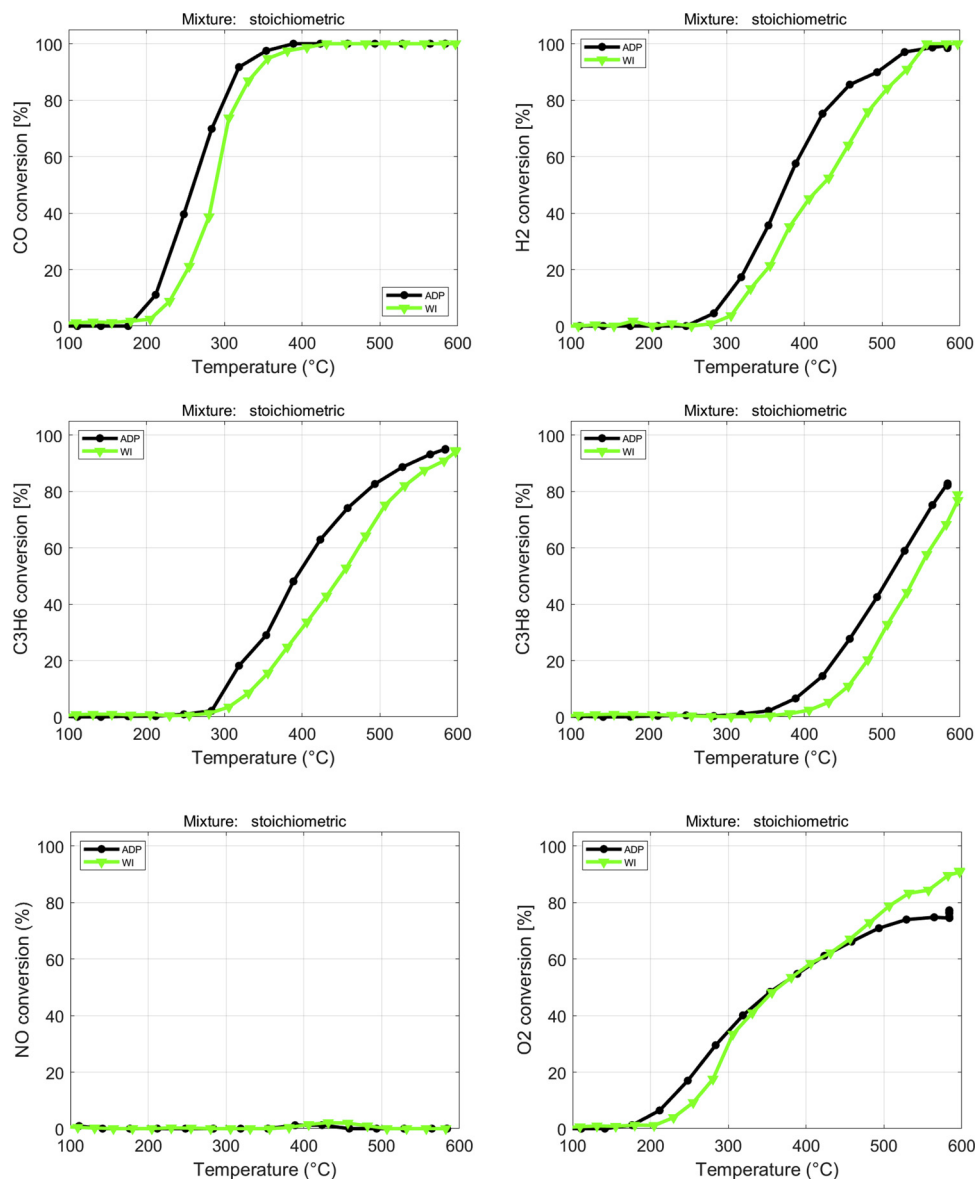


Fig. 8. Single reactants' conversion as a function of temperature, feeding a stoichiometric complex mixture (See Table 2) on 20% copper oxide loading on La_{0.5}Sr_{0.5}CoO₃, synthetized via ADP (black, •) and via WI (green, ▼).

4. Conclusions

In this paper several composite catalysts prepared by depositing CuO on a La_{0.5}Sr_{0.5}CoO₃ powder have been developed aiming at application in TWCs. The nanocomposites have been obtained by means of a new method: Ammonium-driving Deposition Precipitation (ADP). The procedure allows to obtain a high dispersion of the copper oxide. The samples have been characterized by means of X-Ray Photoelectron Spectroscopy, X-Ray Diffraction, Temperature Programmed Reduction, Scanning Electron Microscopy, Energy Dispersive X-Ray analysis, and the obtained results are consistent with a homogeneous deposition of highly dispersed CuO on the surface of the perovskite. XRD shows that copper oxide is deposited on the perovskite surface and do not enter the crystalline cell. However, when the amount of copper deposited increases (in 30 wt% CuO/La_{0.5}Sr_{0.5}CoO₃) it tends to migrate inside grains creating fractures. The deposition of copper oxide increases the reducibility, as confirmed by TPR, affecting also the reactivity. The reactivity in two model reactions, CO oxidation and CO-assisted NO reduction was studied to evaluate the role of the different species. The activity in both reactions increases in the composites. The CO oxidation

starts at much lower temperature with the minimum amount of CuO used (10%); additional Cu is not equally effective. CuO dramatically improves the activity in CO + NO reaction, achieving NO conversion in excess of 60% at 250 °C, and more than 90% at 400 °C. Results with a complex mixture simulating engine exhaust (gasoline) conditions, confirm the significant improvements in activity of the composite. At stoichiometric O₂ we can appreciate the lowering of the temperature required to oxidize CO, H₂, and hydrocarbons to the same extent of bare LSC, approaching comparable composites on LaCoO₃ (with half of the La in the structure). Methane remains very difficult to activate below 500 °C and NO conversion is also very limited with stoichiometric O₂. On the contrary, at fuel-rich conditions (i.e. lack of O₂), the reduction of NO can be quantitative, boosting after the complete consumption of the limited O₂ available, above 400 °C. This interesting result is achieved without modifying the oxidation capacity for CO, H₂, and hydrocarbons; in some case (H₂ and propane), CuO largely improves the oxidation rates, as far as O₂ is available. Apparently, the known limitations on NO reduction rate in the presence of O₂ is confirmed, but the overall performances are quite promising.

The improved dispersion of copper obtained through ADP method

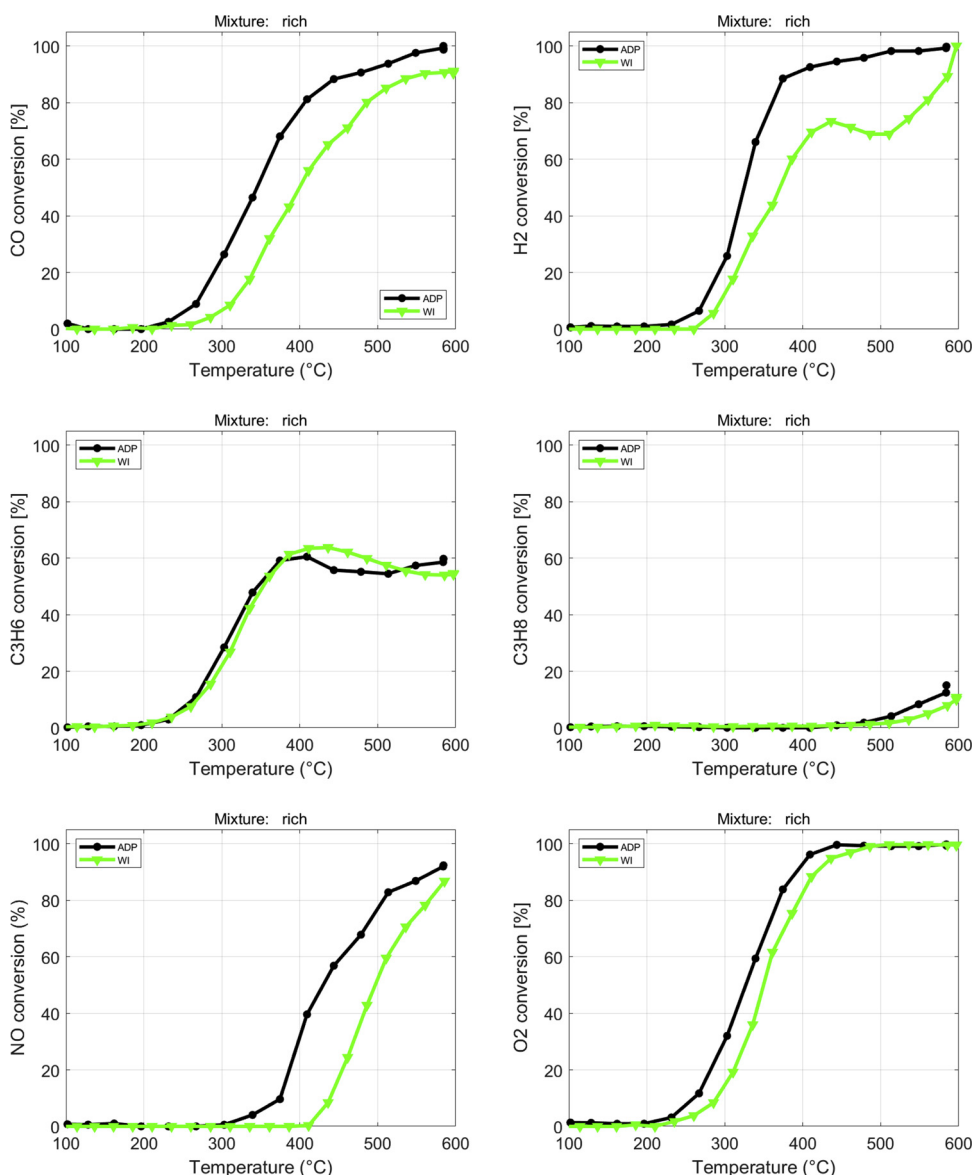


Fig. 9. Single reactants' conversion as a function of temperature, feeding a fuel-rich complex mixture (See Table 2) on 20% copper oxide loading on $\text{La}_{0.5}\text{Sr}_{0.5}\text{CoO}_3$, synthetized via ADP (black, •) and via WI (green, ▼).

leads to a higher reactivity, both in stoichiometric and in rich conditions, compared to the same material prepared via wet impregnation. Notably, NO reduction in oxygen-lean conditions is improved, both as lower ignition temperature (300 °C achieved with ADP sample, against 400 °C with WI) and activity at the same temperature, significantly higher in ADP catalyst.

The obtained results indicate that interesting catalytic performances can be achieved in noble metal-free catalysts by means of high dispersion of copper oxide on the surface of perovskites. Perovskite based nanocomposites can thus be considered a new frontier in sustainable catalysis.

Acknowledgement

The research work was developed in the frame of the H2020 project PARTIAL PGMS ('Development of novel, high performance hybrid TWC/GPF automotive after treatment systems by rational design'; project n° 686086).

References

- [1] W.F. Libby, Promising catalyst for auto exhaust, *Science* 171 (1971) 499–500.
- [2] S.C. Sorenson, J.A. Wronkiewicz, L.B. Sis, G.P. Wirtz, Properties of LaCoO_3 as a catalyst in engine exhaust gases, *Bull. Am. Ceram. Soc.* 53 (1974) 446–449.
- [3] L. Lisi, G. Bagnasco, P. Ciambelli, S. De Rossi, P. Porta, G. Russo, M. Turco, Perovskite-type oxides: II. Redox properties of $\text{LaMn}_{1-x}\text{Cu}_x\text{O}_3$ and $\text{LaCo}_{1-x}\text{Cu}_x\text{O}_3$ and methane catalytic combustion, *J. Solid State Chem.* 146 (1999) 176–183.
- [4] L. Simonot, F. Garin, G. Maire, A comparative study of LaCoO_3 , Co_3O_4 and $\text{LaCoO}_3\text{-Co}_3\text{O}_4$: I. Preparation, characterisation and catalytic properties for the oxidation of CO, *Appl. Catal. B* 11 (1997) 167–179.
- [5] B. Seyfi, M. Baghaha, H. Kazemian, LaCoO_3 nano-perovskite catalysts for the environmental application of automotive CO oxidation, *Chem. Eng. J. Chem. Eng. J.* 148 (2009) 306–311.
- [6] S. Cimino, G. Landi, L. Lisi, G. Russo, Development of a dual functional structured catalyst for partial oxidation of methane to syngas, *Catal. Today* 117 (2006) 454–461.
- [7] N. Guilhaume, M. Primet, Three-way catalytic activity and oxygen storage capacity of perovskite $\text{LaMn}_{0.976}\text{Rh}_{0.024}\text{O}_3+\delta$, *J. Catal.* 165 (1997) 197–204.
- [8] P. Doggali, S. Kusaba, Y. Teraoka, P. Chankapure, S. Rayalu, N. Labhsetwar, $\text{La}_{0.9}\text{Ba}_{0.1}\text{CoO}_3$ perovskite type catalysts for the control of CO and PM emissions, *Catal. Commun.* 11 (2010) 665–669.
- [9] T. Nakamura, M. Misono, Y. Yoneda, Catalytic properties of perovskite-type mixed oxides, $\text{La}_{1-x}\text{Sr}_x\text{CoO}_3$, *Bull. Chem. Soc. Jpn.* 55 (1982) 394–399.
- [10] D. Hari Prasad, S.Y. Park, E.-O. Oh, H. Ji, H.-R. Kim, K.-J. Yoon, et al., Synthesis of nano-crystalline $\text{La}_{1-x}\text{Sr}_x\text{CoO}_3$ perovskite oxides by EDTA-Citrate complexing

- process and its catalytic activity for soot oxidation, *Appl. Catal. A Gen.* 447–448 (2012) 100–106.
- [11] M. Morales, F. Espiell, M. Segarra, Performance and stability of $\text{La}_{0.5}\text{Sr}_{0.5}\text{CoO}_3$ -delta perovskite as catalyst precursor for syngas production by partial oxidation of methane, *Int. J. Hydrogen Energy* 39 (2014) 6454–6461.
- [12] L.A. Isupova, G.M. Alikina, S.V. Tsybulya, N.N. Boldyreva, G.N. Kryukova, I.S. Yakovleva, V.P. Isupov, V.A. Sadykov, Real structure and catalytic activity of $\text{La}_{1-x}\text{Sr}_x\text{CoO}_3$ perovskites, *Int. J. Inorg. Mater.* 3 (2001) 559–562.
- [13] V.V. Srdić, R.P. Omorjan, J. Seydel, Electrocatalytic performances of $(\text{La}, \text{Sr})\text{CoO}_3$ cathode for zirconia-based solid oxide fuel cells, *Mater. Sci. Eng. B* 116 (2005) 119–124 and references therein.
- [14] E.V. Tsipis, E.N. Naumovich, M.V. Patrakeev, A.A. Yaremchenko, I.P. Marozau, A.V. Kovalevsky, J.C. Waerenborgh, V.V. Kharton, Oxygen deficiency, vacancy clustering and ionic transport in $(\text{La}, \text{Sr})\text{CoO}_3-\delta$, *Solid State Ion.* 192 (2011) 42–48.
- [15] Y. Zhang-Steenwinkel, Q. Yu, F.P.F. van Berkel, M.M.A. van Tuel, B. Rietveld, H. Tu, High performance solid-oxide fuel cell: opening windows to low temperature application, *Int. J. Hydrogen Energy* 41 (2016) 5824–5832.
- [16] A. Bieberle-Hütter, M. Søgaard, H.L. Tuller, Electrical and electrochemical characterization of microstructured thin film $\text{La}_{1-x}\text{Sr}_x\text{CoO}_3$ electrodes, *Solid State Ion.* 177 (2006) 1969–1975.
- [17] H. Kozuka, K. Ohbayashi, K. Koumoto, Electronic conduction in La-based perovskite-type oxides, *Sci. Technol. Adv. Mater.* 16 (2015) 026001–026016.
- [18] A. Glisenti, M. Pacella, M. Guiotto, M.M. Natile, P. Canu, Largely Cu-doped $\text{LaCo}_{1-x}\text{Cu}_x\text{O}_3$ perovskites for TWC: toward new PGM-free catalysts, *Appl. Catal. B: Environ.* 180 (2016) 94–105.
- [19] G. Perin, J. Fabro, M. Guiotto, Q. Xin, M.M. Natile, P. Cool, P. Canu, A. Glisenti, Cu@ LaNiO_3 based nanocomposites in TWC applications, *Appl. Catal. B Environ.* 209 (2017) 214–227.
- [20] M. Navarro, M.A. Peña, J.L.G. Fierro, Hydrogen production reactions from carbon feedstocks: fossil fuels and biomass, *Chem. Rev.* 107 (2007) 3952–3991.
- [21] C.-Y. Lu, W.-C. Chang, M.-Y. Wey, Cu/CeO_2 catalysts prepared with different cerium supports for CO oxidation at low temperature, *Mater. Chem. Phys.* 141 (2013) 512–518.
- [22] S. Zeng, Y. Wang, S. Ding, J.J.H.B. Sattler, E. Borodina, L. Zhang, B.M. Weckhuysen, H. Su, Active sites over CuO/CeO_2 and inverse CeO_2/CuO catalysts for preferential CO oxidation, *J. Power Sources* 256 (2014) 301–311.
- [23] C. Tang, J. Sun, X. Yao, L. Liu, C. Ge, F. Gao, L. Dong, Efficient fabrication of active $\text{CuO}/\text{CeO}_2/\text{SBA}-15$ catalysts for preferential oxidation of CO by solid state impregnation, *Appl. Catal. B: Environ.* 146 (2014) 201–212.
- [24] A.K. Ahmed, A.A. Zuhairi, M.A. Rahman, Recent development in catalytic technologies for methanol synthesis from renewable sources: a critical review, *Renew. Sust. Energy Rev.* 44 (2015) 508–518.
- [25] S.G. Jadhav, P.D. Vaidya, B.M. Bhanage, J.B. Joshi, Catalytic carbon dioxide hydrogenation to methanol: a review of recent studies, *Chem. Eng. Res. Des.* 92 (2014) 2557–2567.
- [26] I. Rodriguez-Ramos, A. Guerrero-Ruiz, M.L. Rojas, J.L.G. Fierro, Dehydrogenation of methanol to methyl formate over copper-containing perovskite-type oxides, *Appl. Catal. A* 68 (1991) 217–228.
- [27] G. Perin, A. Glisenti, Perovskites as alternatives to noble metals in automotive exhaust abatement: activation of oxygen on LaCrO_3 and LaMnO_3 , *Top. Catal.* (December) (2018), <https://doi.org/10.1007/s11244-018-1120-1>.
- [28] M. Pacella, A. Garbujo, J. Fabro, M. Guiotto, Q. Xin, M.M. Natile, P. Canu, P. Cool, A. Glisenti, PGM-free $\text{CuO}/\text{LaCoO}_3$ nanocomposites: new opportunities for TWC application, *Appl. Catal. B: Environ.* 227 (2018) 446–458.
- [29] X. Guo, A. Yin, W.L. Dai, One pot synthesis of ultra-high copper contented Cu/SBA-15 material as excellent catalyst in the hydrogenation of dimethyl oxalate to ethylene glycol, *Catal. Lett.* 132 (2009) 22–27.
- [30] C. Marcilly, P. Courty, B. Delmon, Preparation of highly dispersed mixed oxides and oxide solid solutions by pyrolysis of amorphous organic precursors, *J. Am. Ceram. Soc.* 53 (1970) 56–57.
- [31] D.A. Shirley, High resolution X-Ray Photoemission spectrum of the valence band of gold, *Phys. Rev. B* 5 (1972) 4709–4714.
- [32] J.F. Moulder, W.F. Stickle, P.E. Sobol, K.D. Bomben, Handbook of X-ray photoelectron spectroscopy, in: J. Chastain (Ed.), *Physical Electronics*, 1992 Eden Prairie, MN.
- [33] D. Briggs, J.C. Riviere, D. Briggs, M.P. Seah (Eds.), *Practical Surface Analysis*, Wiley, New York, 1983.
- [34] M. Guiotto, M. Pacella, G. Perin, A. Iovino, N. Michelon, M.M. Natile, A. Glisenti, P. Canu, Washcoating vs. Direct synthesis of LaCoO_3 on monoliths for environmental applications, *Appl. Catal. A Gen.* 499 (2015) 146–157.
- [35] X. Cheng, E. Fabbri, M. Nachtegaal, I.E. Castelli, M. El Kazzi, R. Haumont, N. Marzari, T.J. Schmidt, Oxygen evolution reaction on $\text{La}_{1-x}\text{Sr}_x\text{CoO}_3$ perovskites: a combined experimental and theoretical study of their structural, electronic, and electrochemical properties, *Chem. Mater.* 27 (2015) 7662–7672.
- [36] NIST XPS Database 20, Version 3.4 [Web Version].
- [37] M.M. Natile, F. Poletto, A. Galenda, A. Glisenti, T. Montini, L. De Rogatis, P. Fornasiero, $\text{La}_{0.6}\text{Sr}_{0.4}\text{Co}_{1-y}\text{Fe}_y\text{O}_3-\delta$ perovskites: influence of the Co/Fe atomic ratio on properties and catalytic activity toward alcohol steam-reforming, *Chem. Mater.* 20 (2008) 2314–2327.
- [38] A. Galenda, M.M. Natile, V. Krishnan, H. Bertagnolli, A. Glisenti, LaSrCoFeO and $\text{Fe}_2\text{O}_3/\text{LaSrCoFeO}$ powders: synthesis and characterization, *Chem. Mater.* 19 (2007) 2796–2808.
- [39] A. Galenda, M.M. Natile, L. Nodari, A. Glisenti, $\text{La}_{0.8}\text{Sr}_{0.2}\text{Ga}_{0.8}\text{Fe}_{0.2}\text{O}_3-\delta$: influence of the preparation procedure on reactivity toward methanol and ethanol, *Appl. Catal. B: Environ.* 97 (2010) 307–322.
- [40] M.A. Peña, J.L.G. Fierro, Chemical structures and performance of perovskite oxides, *Chem. Rev.* 101 (2001) 1981–1988.
- [41] R. Lago, G. Bini, M.A. Pena, J.L.G. Fierro, Partial oxidation of methane to synthesis gas using LnCoO_3 perovskites as catalyst precursors, *J. Catal.* 167 (1997) 198–209.
- [42] J.L.G. Fierro, Structure and composition of perovskite surface in relation to adsorption and catalytic properties, *Catal. Today* 8 (1990) 153–174.
- [43] L. Bedel, A.C. Roger, C. Estournes, A. Kiennemann, CoO from partial reduction of $\text{La}(\text{Co}, \text{Fe})\text{O}_3$ perovskites for Fischer-Tropsch synthesis, *Catal. Today* 85 (2003) 207–218.
- [44] L.B. Sis, G.P. Wirtz, S.C. Sorenson, Structure and properties of reduced LaCoO_3 , *J. Appl. Phys.* 44 (1973) 5553–5559.
- [45] B. Echchahed, S. Kaliaguine, H.S. Almadari, Well dispersed CoO by reduction of LaCoO_3 perovskite, *Int. J. Chem. React. Eng.* 4 (2006) A29.
- [46] J.L.G. Fierro, M. Loacono, M. Inversi, P. Porta, R. Lavecchia, F. Cioci, A study of anomalous temperature-programmed reduction profiles of Cu_2O , CuO and CuO-ZnO catalysts, *J. Catal.* 148 (1994) 709–721.
- [47] Q. Xin, A. Papavasiliou, N. Boukos, Nikos A. Glisenti, J.P.H. Li, Y. Yang, C.J. Philippopoulos, E. Poulakis, F.K. Katsaros, V. Meynen, P. Cool, Preparation of CuO/SBA-15 catalyst by the modified ammonia driven deposition precipitation method with a high thermal stability and an efficient automotive CO and hydrocarbons conversion, *Appl. Catal. B Environ.* 223 (2018) 103–115 and references therein.
- [48] Q. Xin, A. Glisenti, C. Philippopoulos, E. Poulakis, M. Mertens, J.L. Nyalosaso, V. Meynen, P. Cool, Comparison between a water-based and a solvent-based impregnation method towards dispersed CuO/SBA-15 catalysts: texture, structure and catalytic performance in automotive exhaust gas abatement, *Catalysts* 6 (2016), <https://doi.org/10.3390/catal6100146> Art 164.
- [49] L. Kundakovic, M. Flytzani-Stephanopoulos, Reduction characteristics of copper oxide in cerium and zirconium oxide systems, *Appl. Catal. A Gen.* 171 (1998) 13–29.
- [50] Z. Wu, H. Zhu, Z. Qin, H. Wang, J. Ding, L. Huang, J. Wang, CO preferential oxidation in H_2 rich stream over a CuO/CeO_2 catalyst with high H_2O and CO_2 tolerance, *Fuel* 104 (2013) 41–45.
- [51] S. Zeng, Y. Wang, S. Ding, J.J.H.B. Sattler, E. Borodina, L. Zhang, B.M. Weckhuysen, H. Su, Active sites over CuO/CeO_2 and inverse CeO_2/CuO catalysts for preferential CO oxidation, *J. Power Sources* 256 (2014) 301–311.
- [52] C.A. Chagas, E.F. de Souza, R.L. Manfro, S.L. Landi, M.M.V.M. Souza, M. Schmal, Copper as promoter of the NiO-CeO_2 catalyst in the preferential CO oxidation, *Appl. Catal. B Environ.* 182 (2016) 257–265.
- [53] C. He, Y. Yu, Q. Shen, J. Chen, N. Qiao, Catalytic behavior and synergistic effect of nanostructured mesoporous CuO-MnO_x-CeO_2 catalysts for chlorobenzene destruction, *Appl. Surf. Sci.* 297 (2014) 59–69.
- [54] J.-L. Cao, Y. Wang, G. Sun, Z.-Y. Zhang, $\text{CuO/Ce}_{x}\text{Sn}_{1-x}\text{O}_2$ catalysts: synthesis, characterization, and catalytic performance for low-temperature CO oxidation, *Transition Met. Chem.* 36 (2011) 107–112.
- [55] Z. Wu, H. Zhu, Z. Qin, H. Wang, L. Huang, J. Wang, Preferential oxidation of CO in H_2 -rich stream over $\text{CuO/CE}_{1-x}\text{Ti}_x\text{O}_2$, *Appl. Catal. B Environ.* 98 (2010) 204–212 and references therein.
- [56] L. Dong, Y. Tang, B. Li, L. Zhou, F. Gong, H. He, B. Sun, C. Tang, F. Gao, L. Dong, Influence of molar ratio and calcination temperature on the properties of $\text{Ti}_{x}\text{Sn}_{1-x}\text{O}_2$ supporting copper oxide for CO oxidation, *Appl. Catal. B Environ.* 180 (2016) 451–462.
- [57] M.F. Luo, J.M. Ma, J.Q. Lu, Y.P. Song, Y.J. Wang, High-surface area CuO-CeO_2 catalysts prepared by a surfactant-templated method for low-temperature CO oxidation, *J. Catal.* 246 (2007) 52–59.
- [58] W.P. Dow, T.J. Huang, Effect of oxygen vacancy of yttria stabilized zirconia support on carbon monoxide oxidation over copper catalyst, *J. Catal.* 147 (1994) 322–332.
- [59] M.M. Natile, G. Eger, P. Batocchi, F. Mauvy, A. Glisenti, Strontium and copper doped LaCoO_3 New cathode materials for solid oxide fuel cells? *Int. J. Hydrogen Energy* 42 (2017) 1724–1735.
- [60] N. Tien Thao, H. Almadari, M.H. Zahedi-Niaki, S. Kaliaguine, $\text{LaCo}_{1-x}\text{Cu}_x\text{O}_3-\delta$ perovskite catalysts for higher alcohol synthesis, *Appl. Catal. A Gen.* 311 (2006) 204–212.
- [61] N. Tien Thao, H. Almadari, S. Kaliaguine, Characterization and reactivity of nanoscale $\text{La}(\text{Co}, \text{Cu})\text{O}_3$ perovskite catalyst precursors for CO hydrogenation, *J. Sol. State. Chem.* 181 (2008) 2006–2019.
- [62] J.A. Onrubia, B. Pereda-Qyo, U. De-La-Torre, J.R. González-Velasco, Key factors in Sr-doped LaBO_3 ($B = \text{Co}$ or Mn) perovskites for NO oxidation in efficient diesel exhaust purification, *Appl. Catal. B Environ.* 213 (2017) 198–210.
- [63] P. Mars, D.W. van Krevelen, Oxidations carried out by means of vanadium oxide catalysts, *Chem. Eng. Sci.* 3 (1954) 41–59, [https://doi.org/10.1016/S0009-2509\(54\)80005-4](https://doi.org/10.1016/S0009-2509(54)80005-4).
- [64] J.L.G. Fierro, L.G. Tejada, Kinetics and mechanism of CO oxidation on LaCoO_3 , *Z. Phys. Chem.* 1981 (1981) 249–257.
- [65] D. Pinto, A. Glisenti, Pulsed Chemisorption on Perovskite: a Kinetic Approach to Go Inside the Effect of Dopants, In press on *Catalysis Science and Technology* (2019), <https://doi.org/10.1039/C9CY00210C>.
- [66] R. Zhang, A. Villanueva, H. Almadari, S. Kaliaguine, Reduction of NO by CO over nanoscale $\text{LaCo}_{1-x}\text{Cu}_x\text{O}_3$ and $\text{LaMn}_{1-x}\text{Cu}_x\text{O}_3$ perovskites, *J. Mol. Catal. A* 258 (2006) 22–34.
- [67] R. Zhang, A. Villanueva, H. Almadari, S. Kaliaguine, Catalytic reduction of NO by propane over $\text{LaCo}_{1-x}\text{Cu}_x\text{O}_3$ perovskites synthesized by reactive grinding, *Appl. Catal. B Environ.* 64 (2006) 220–233.
- [68] G. Centi, S. Perathoner, L. Dall’Olio, Modification of the surface reactivity of Cu-MFI during chemisorption and transformation of the reagents in the selective reduction of NO with propane and O_2 , *Appl. Catal. B Environ.* 7 (1996) 359–377.
- [69] E.M. Sadovskaya, A.P. Suknev, L.G. Pinaeva, V.B. Goncharov, B.S. Balzhinimaev,

- C. Chupin, C. Mirodatos, Mechanism and kinetics of the selective NO reduction over Co-ZSM-5 studied by the SSITKA technique, *J. Catal.* 201 (2001) 159–168.
- [70] E.M. Sadovskaya, A.P. Suknev, L.G. Pinaeva, V.B. Goncharov, B.S. Bal'zhinimaev, C. Chupin, J. Pérez-Ramírez, C. Mirodatos, Mechanism and kinetics of the selective NO reduction over Co-ZSM-5 studied by the SSITKA technique 2. Reactivity of NOx-adsorbed species with methane, *J. Catal.* 225 (2004) 179–189.
- [71] J.M.D. Tascón, L.G. Tejeda, C.H. Rochester, Surface interactions of NO and CO with LaMO₃ oxides, *J. Catal.* 95 (1985) 558–566.
- [72] C. Chupin, A.C. van Veen, M. Konduru, J. Després, C. Mirodatos, Identity and location of active species for NO reduction by CH₄ over Co-ZSM-5, *J. Catal.* 241 (2006) 103–114.
- [73] G. Centi, S. Perathoner, Nature of active species in copper-based catalysts and their chemistry of transformation of nitrogen oxides, *Appl. Catal. A Gen.* 132 (1995) 179–259.
- [74] C. Zhou, X. Liu, C. Wu, Y. Wen, Y. Xue, R. Chen, Z. Zhang, B. Shan, H. Yin, W. Guo Wang, NO oxidation catalysis on copper doped hexagonal phase LaCoO₃: a combined experimental and theoretical study, *Phys. Chem. Chem. Phys.* 16 (2014) 5106–5112.